Open Access

REE-Rich Aeschynite in Apatite-Dolomite Carbonatite, Eastern Oman Mountains

Sobhi Nasir[*,1], Thomas Theye[2] and Hans-Joachim Massonne[2]

[1]*Department of Earth Sciences, Sultan Qaboos University, P.O.Box 36, 123 Al-Khod, Oman;* [2]*Institut für Mineralogie und Kristallchemie, Universität Stuttgart, Azenbergstr. 18, D-70174 Stuttgart, Germany*

Abstract: Aeschynite-(Ce) and nioboaeschynite-(Ce**)** occur as late stage minerals in apatite-dolomite-carbonatite in the eastern Oman Mountains. Micro Raman spectroscopic analysis confirmed that the analysed minerals are aeschynites. Microprobe analyses revealed that the concentrations of REE_2O_3 are very high, ranging from 33 to 43 wt.%. The chondrite-normalized REE patterns are LREE-rich. La/Nd ratios vary in the range ~ 0.4 to 5.8. Several complex substitution mechanisms have been proposed for aeschynite, which are mainly governed by charge balance considerations, with $(OH)^- + Ti^{4+} = O^{2-} + (Nb^{5+}, Ta^{5+})$ being the most prominent one. In addition, the composition of aeschynite is affected by local compositional parameters.

Keywords: Aeschynite group, rare earth elements, compositional variation, carbonatite, Oman, Raman spectroscopy.

INTRODUCTION

The euxenite- and aeschynite-group minerals (REE, Y, Ca, Th) $(Ti, Nb)_2$ $(O, OH, F)_6$ are two of the few mineral series in which compositions range between light rare-earth element (LREE) and heavy rare-earth element (HREE) including yttrium as well as niobium and titanium dominated members. This characteristic is mainly controlled by the crystal chemistry of euxenite and aeschynite, the structure of which is characterized by polyhedra of suitable sizes to host both LREE and Y+HREE [1]. However, euxenite-group minerals are often HREE-dominat, while aeschynite-group minerals are usually LREE-dominant [2,3]. Generally, aeschynite consists of a three-dimensional framework of B octahedra (B = Ti, Nb, Ta, W, Fe^{3+}) and a variety of large A cations (A = Y, REE, Zr, Th, U, Ca, Sr) placed in the tunnels of connected vacancies [1]. There are various coupled substitutions concerning both A and B sites [e.g., 4] such as $(Th^{4+}, U^{4+}) + Ti^{4+} = Y^{3+} + (Nb^{5+}, Ta^{5+})$, $REE^{3+} + Ti^{4+} = Ca^{2+} + (Nb^{5+}, Ta^{5+})$ and $(OH)^- + Ti^{4+} = O^{2-} + (Nb^{5+}, Ta^{5+})$.

Although the aeschynite-group minerals are typically only accessories in rocks they are common in REE enriched granites. Aeschynite mostly occurs as late-stage, often metamict mineral in granitic and syenitic pegmatites, hydrothermal deposits, carbonatites and kimberlites [e.g., 5-10]. Aeschynite is commonly found at a metamict state as a consequence of the alpha-decay associated with the usually high Th and U contents [e.g. 9]

Aeschynite group minerals were identified as the principal REE-bearing minerals in a newly found carbonatite occurrence at the Sal area, eastern Oman (Fig. **1**). The aim of this study is to characterize the aeschynite group minerals within these carbonatites and to discuss their crystal chemistry.

GEOLOGICAL SETTING

Carbonatites, kimberlites and aillikite lamprophyres have been recently discovered in the Batain Nappes area in eastern Oman [11,12]. The corresponding diatremes, dykes and plugs belong to an Upper Jurassic to lower Cretaceous alkaline suites associated with regional crustal extension and major uplift in the Oman Mountain range that finally resulted in the formation of the eastern Oman ophiolite [11,12]. Among the new carbonatite occurrences is the recently discovered carbonatite of this study, which is situated in the eastern part of Oman, in the vicinity of Sal village (Fig. **1**). The economic value of the newly discovered carbonatites and kimberlites in eastern Oman will be discussed in a separate paper.

Ar-Ar whole rock age dating on the Sal carbonatites gave an intrusion age between 379 and 387 $\pm$ 5 Ma (Nasir et al. in preparation). The Sal carbonatites are partly covered by the Triassic Sal Formation within the Batain mélange. The Batain mélange consists predominantly of Triassic to Cretaceous allochthonous marine sediments and ophiolite fragments of the eastern Oman Mountains. These rocks are unconformably overlain by a Maastrichtian and lower Tertiary shelf sequence; they have been deformed during mid to late Tertiary extensional events and Tertiary volcanism associated with the major uplift of the Oman mountain range [13].

The discovered carbonatites are confined to the extreme eastern corner of Oman around the Jebel Ja'alan basement block (Fig. **1**). The Late Proterozoic and Phanerozoic sedimentary rocks exposed in central and eastern Oman show evidence of several unconformities that record intermittent structural high and contemporaneous basin subsidence [14].

*Address correspondence to this author at the Department of Earth Sciences, Sultan Qaboos University, P.O.Box 36, 123 Al-Khod, Oman;.
E-mail: sobhi@squ.edu.om

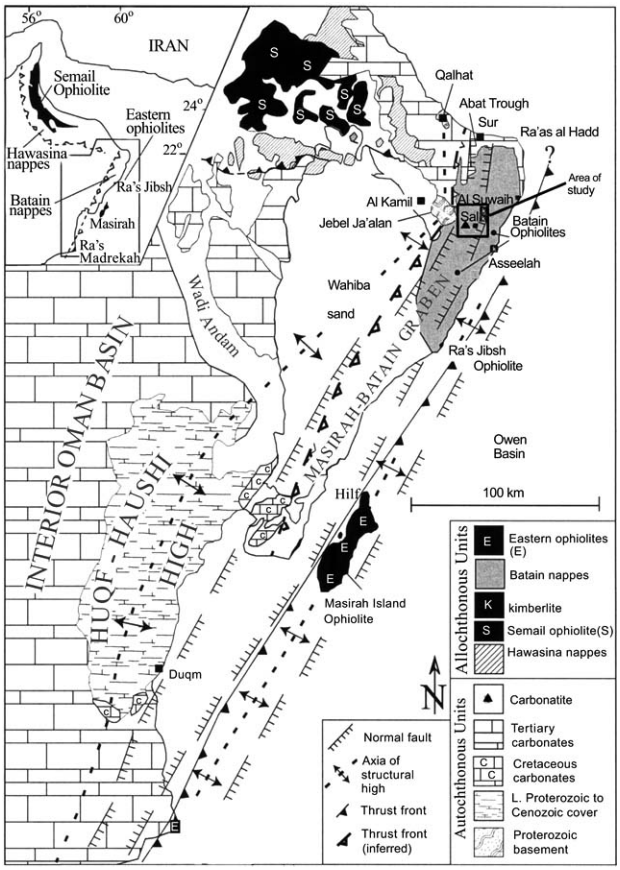

Fig. (1). Location map of the study area.

This structural high is a part of the Hqf-Haushi Uplift, which is bounded to the northeast by NNE oriented extensional faults. The Huqf-Haushi Uplift exposes Pre-Cambrian crystalline basement at Jabal Ja'alan and at Wadi Sal, eastern Oman. In general, Cambrian to Permian magmatic activity in Oman was closely related to major fracture zones associated with several rift cycles. However, volcanic roks of the Cambrian and Ordovician [15] and the Middle Permian [16] exhibit trace element and isotopic characteristics of plume-related magmas. The Devonian age of the carbonatites at Wadi Sal is likely to be the result of either a separate mantle upwelling or reactivation of the same instability during Devonian tectonic events. The carbonatites are exposed along NS to EW faults along the flank of the earlier rifted basins and parallel to the major tectonic structure in the region, suggesting that the faults are extensional, and have acted as conduits for the carbonatite magma. The carbonatite at Wadi Sal provides the first clear evidence of a pulse of rift-shoulder uplift in eastern Oman during the Devonian (Nasir et al., in prep). Our the data show that these events are consistent with a period of break-up of eastern Gondwanaland.

SAMPLES AND ANALYTICAL METHODS

The carbonatites are exposed as conical hills or elliptical plugs that rise to 5-20 m above the surrounding rocks of the Pre-Cambrian basement and allochthonous rocks of the Batain nappes. In most cases the carbonatites have intrusive contacts with the basement rocks. Aeschynite-bearing Carbonatites were sampled from one locality in the western side of Wadi Sal. The other carbonatite localities occur in the eastern part of Wadi Sal at a distance of about 20 km from the western carbonatite locality. These carbonatites are phlogopite-rich, Ce-monazite-bearing and devoid of aeschynite. The aeschynite-bearing carbonatites are spotted, yellowish-grey to dark grey in color, and fine-grained. They are mainly composed of dolomite (40-45 vol.%), calcite (10-15 vol. %), fluorapatite (20-30 vol.%) and magnetite partially rimmed by hematite (10-20 vol.%). The following accessory minerals were identified by electron microprobe analysis: aeschynite-group minerals, barite, baddeleyite, thorianite, Nb-rutile, strontianite, and intergrowths of alteration products such as limonite, chlorite and serpentine (Nasir et al., in prep). Aeschynite-group minerals are omnipresent accessory phases in our samples and occur as anhedral crystals of variable shape and small size (1 to 10 um, Fig. **2**). The grains are mostly interstitial within the carbonate mineral

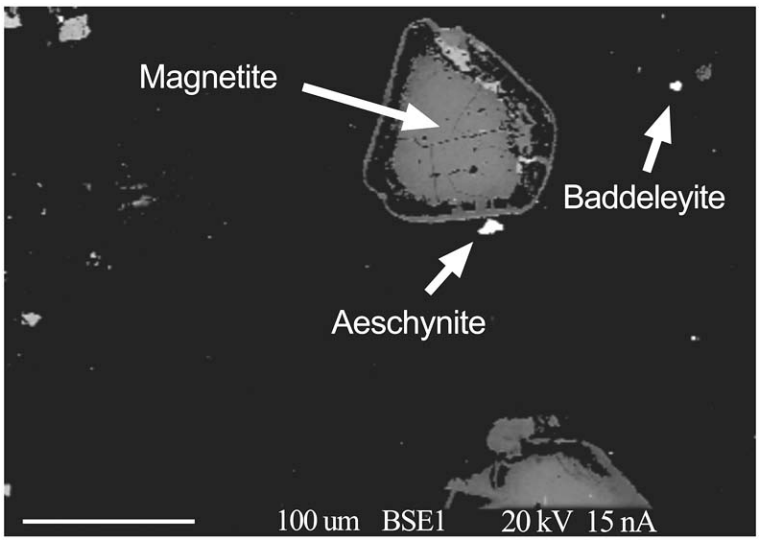

Fig. (2). Backscattered electron image of aeschynite from the Sal area. Black area is carbonate and apatite.

groundmass or occur as small grains epitaxially growing on the grain boundary of magnetite, partly at the interface to the hematite rims (Fig. **2**). These structural features point to a relatively late formation of aeschynite with respect to euhedral magnetite.

The chemical composition of aeschynite was examined by WDS electron probe microanalysis performed with a CAMECA SX100 at the Institute of Mineralogy, Stuttgart University. The analyses were undertaken with an accelerating voltage of 15 kV and 30 nA beam current. The following analytical lines and crystals were used for the analysis:

F Ka	TAP	Fluorite	(0.12 wt.%)
Si Ka	TAP	orthoclase	(0.01 wt.%)
P Ka	PET	LaPO4	(0.04 wt.%)
Ca Ka	PET	diopside	(0.02 wt.%)
Ti Ka	PET	rutile	(0.02 wt.%)
Mn Ka	LIF	rhodonite	(0.04 wt.%)
Fe Ka	LIF	Fe2O2	(0.03 wt.%)
Sr La	TAP	celestite	(0.03 wt.%)
Y La	TAP	glass	(0.03 wt.%)
Zr La	PET	Zr	(0.12 wt.%)
Nb La	PET	Nb	(0.05 wt.%)
La La	LIF	phosphate	(0.20 wt.%)
Ce La	LIF	phosphate	(0.27 wt.%)
Pr Lb	LIF	glass	(0.20 wt.%)
Nd La	LIF	glass	(0.09 wt.%)
Sm La	LIF	glass	(0.11 wt.%)
Eu La	LIF	glass	(0.13 wt.%)
Gd Lb	LIF	glass	(0.15 wt.%)
Dy Lb	LIF	glass	(0.16 wt.%)
Er Lb	LIF	glass	(0.13 wt.%)
Yb La	LIF	glass	(0.11 wt.%)
Ta Ma		Ta	(0.05 wt.%)
W Ma	TAP	CaWO4	(0.04 wt.%)
Pb Mb	PET	PbTe	(0.13 wt.%)
Th Ma		glass	(0.09 wt.%)
U Mb		glass	(0.09 wt.%)

Counting time for all elements was 60 seconds both on peak and on background positions. The estimated detection limits are in the range of 0.1 to 0.2 wt.% for REE, Pb, Zr, and F, and between 100 and 1000 ppm for the other elements. For the positions of background measurement offsets in case of REE and their peak interference, we followed the recommendations by Reed and Buckley [17]. A focused beam was applied due to the small size of the aeschynite grains.

The chemical compositions of aeschynite may be close to those of euxenite and minerals of the pyrochlore group [18]. Therefore, it is difficult to verify the presence of aeschynite on the basis of electron microprobe analyses only, and an additional method is required. The aeschynite grains are too small (< 10 ! m) and associated with magnetite. Accordingly, it was not possible to separate these grains for X-ray diffraction analysis. Therefore, we applied micro Raman spectroscopy using a high resolution Witec CRM200 spectrometer. The Raman microscope is equipped with a frequency doubled Nd-YAG laser (523 nm). Scattered Raman light was collected in 180° backscattering geometry, and dispersed with a grading of 600 groves/mm. A 100x objective lens with a numerical aperture of 0.9 was used.

RESULTS

Raman spectra of the phases under consideration have been acquired from several grains of two different samples of the Sal carbonatite. All collected spectra for this phase show the same peak positions and relative intensity distributions. A sample spectrum is shown in Fig. (**3a**). The main bands of aeschynite are mostly pronounced in the wave number region from 200 to 550 cm^{-1}, which is suitable for fingerprint recognition of the mineral phases with the aeschynite structure. The acquired Raman spectrum of aeschynite from the Sal occurrence was compared with a reference Raman spectrum of aeschynite provided by the Physics Department of the University of Parma, Italy (http://www.fis.unipr.it/phevix/ramandb.html, Aeschynite2). It can be seen that the coincidence is best for the peak position (band at 265-355 $cm^{"1}$ and at 854–857 $cm^{"1}$) with the reference spectrum (Fig. **3b**) is very good, confirming that the investigated minerals are aeschynite. The spectra exhibit a broad peak in the 4000-3200 $cm^{"1}$ region due to the OH stretching (Fig. **3a**).

Microprobe spot analyses of aeschynite from the Sal carbonatite were performed on 21 individual crystals (Table **1**). No significant zonation has been detected within the analysed grains; probably the grain sizes are too small to detect zonation by means of an electron microprobe. Concentrations of Na, W, P, Sr, U, Th, and Pb were always below detection limit. The application of canonical discrimination analysis for (Y, REE, U, Th) - (Nb, Ta, Ti) oxide minerals [15] also suggests that the analyzed minerals belong to the aeschynite or euxenite groups (Fig. **4**). Because of the high LREE contents of the analyzed aeschynite, CV1 extends to a very high value of 14 (Fig. **4**). In addition, all analyses clearly fulfill the tentative criterion for aeschynite group minerals LREE > 0.326 TiO_2 – 0.060 Nb_2O_5 + 3.1 (wt.%), whereas for euxinites the converse applies [18].

The analyses of aeschynite are normalized to 3 cations [e.g. 3]. The water content was calculated according to OH= (6 - O* - F) * 2, with O* being stoichiometric oxygen derived from the cations, corrected for the F content. The resulting formula is close to ideal AB_2X_6 (*A*= REE, Y, Ca, Mn, Zr, Y; *B* = Si, Nb, Ta, Ti, Fe^{3+}, *X* = O, OH, F).

According to the structural investigations of Bonazzi *et al.* [9], the maximum value for the (OH) : O ratio should be 1:5. Most analyses scatter around 1 OH per formula unit.

The analyzed aeschynite-group minerals of the Sal carbonatite generally show high REE contents of 33 to 43 wt.% oxide in comparison to worldwide occurrences, which range

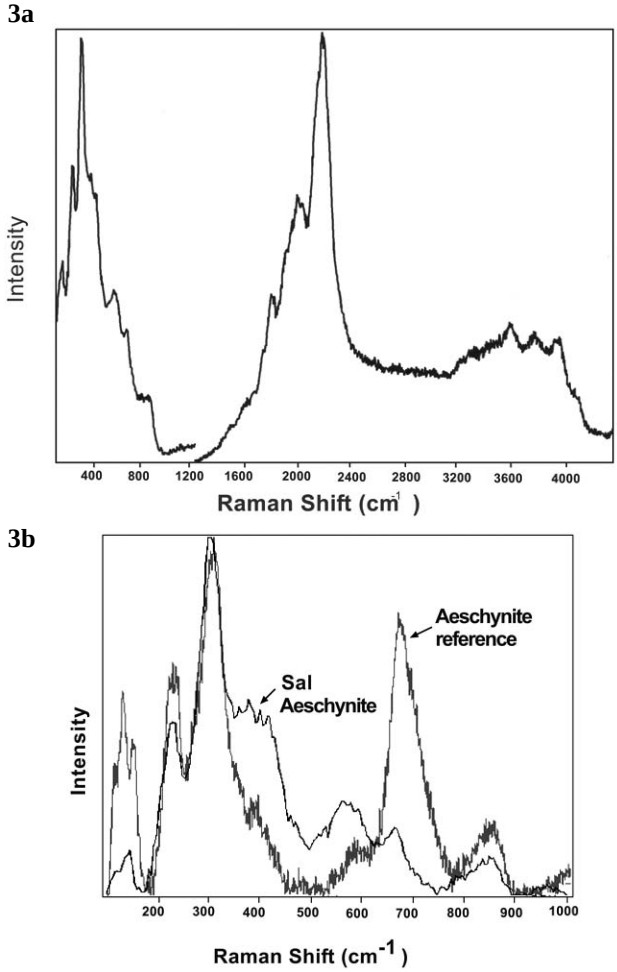

Fig. (3). (**a**) Raman spectrum (raw data) of the aeschynite from the Sal carbonatite. (**b**) The peak positions of the Raman spectrum of the Sal aeschynite in comparison with an aeschynite reference spectrum, provided by the Physics Department of the University of Parma, Italy. Both spectra are corrected for background intensity.

between 16 wt.% [2,6] to 40 wt.% REE oxide [e.g. 19]. On the whole, the chemical composition of the aeschynite-(Ce) from Wadi Sal is close to that of the mineral from Bayan Obo, China [3] (Table **2**). The Nb/(Nb+Ti) ratio varies between 0.0 and 0.6. According to the REE-nomenclature system of Bayliss and Levinson [20] and the interpretation of the 50% rule in multiple solid solution series by the CNMMN [21], two species in the studied samples can be identified as shown in Fig. (**5**). These are: aeschynite-(Ce) and Nb-aeschynite-(Ce).

The A site is almost completely occupied by REE including Y, with a clear predominance of LREE. The most abundant cation present in this site is Ce. In addition to REE and Y, minor Ca is present, up to 0.15 a.p.f.u. Zr is present in small but significant amounts (up to 0.1 cations p.f.u.). The compositions under consideration are in accordance with the literature data [18], according to which LREE are mostly enriched in aeschynite-(Ce), whereas Nb-aeschynite-(Ce) is mostly characterized by higher contents of HREE and Y (Fig. **6b**).

The B site is mostly occupied by the small cations Ti and Nb, with predominance of either Ti or Nb. Smaller quantities

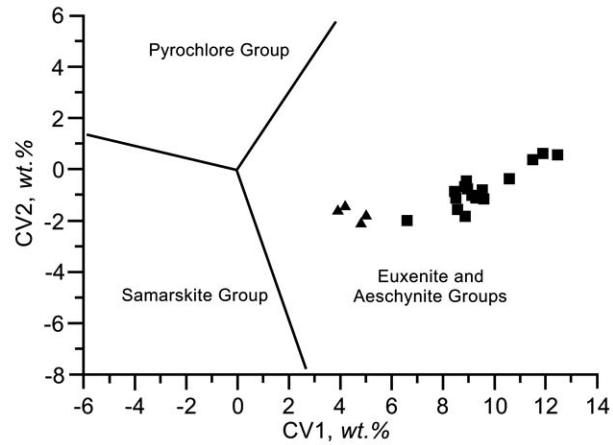

Fig. (4). Canonical discriminant analyses of (Y, REE, U, Th) - (Nb, Ta, Ti) oxide minerals after Ecrit [18]. CV1 = 0.245 Na + 0.106 Ca + 0.077 Fe* + 0.425 Pb + 0.220 Y + 0.280 LREE + 0.137 HREE + 0.100 U + 0.304 Ti + 0.097 Nb + 0.109 Ta – 12.81 (oxide wt.%); CV2 = 0.102 Na - 0.113 Ca - 0.371 Fe* - 0.167 Pb - 0.395 Y - 0.280 LREE - 0.265 HREE - 0.182 U - 0.085 Ti - 0.166 Nb - 0.146 Ta + 17.29 (oxide wt.%). Square: aeschynite-(Ce), triangle: Nb-aeschynite-(Ce).

of iron are also present. Ta_2O_5 plays only a subordinate role (0.2 wt.% in average). The measured SiO_2 content is in the range of 0.1 to 0.7 wt.%. For the highest values of Si, however, a contribution of silicate minerals in the vicinity of the small aeschynite can not be ruled out. Fig. (**7**) shows a diagrammatic representation of the cation population in the B-site.

DISCUSSION

The structure configuration of aeschynite allows for complex cation substitution to occur with variations in both ionic size and charge. In the aeschynites from Sal, Ti correlates negatively with Nb, Zr, Ca, Nd, and Sm, and correlates positively with La, Ce, and OH (Fig. **6a, b**).

A clear negative correlation between Nb and Ti is a result that these two elements are the two stoichiometric species in the B site (Table **3**, Fig. **6a**). However, because of the different charge of Ti^{4+} and Nb^{5+}, a mechanism to maintain the charge balance is required. The substitution mechanism $Ti_1(OH)_1Nb_{-1}O_{-1}$ is suggested, because the calculated OH values also correlate with Ti. The substitution may be generalized by an exchange vector such as $(LREE)_1Ti_{1-}(OH)_1(HREE,Y)_{-1}Nb_{-1}O_{-1}$, because Ti-rich aeschynite is enriched with LREE, whereas for Nb-rich species the converse applies.

An additional B site element that requires charge balance is Fe^{3+} (present up to 0.25 a.p.f.u.). Because there are no other high charge cations such as Th or U present in sufficient amounts in the analyzed aeschynite, it can be expected that charge balance is maintained by $Ti_1O_1Fe^{3+}_{-1}(OH)_{-1}$ substitution or by an intra-B site substitution such as $Fe^{3+}_1Nb_1Ti_{-2}$. Correlation of Fe^{3+} with either Ti or (OH), however, shows no clear trend. Yang *et al*. [3] also found that when Ti largely prevails on Nb + Ta, the amounts of actinides may not be sufficient for charge balance of the formula and the substitution of hydroxyl group for oxygen atoms is required.

Table 1. Electron Microprobe Analysis of Aeschynite Group Minerals from the Sal Carbonatite

Type	**Aeschynite-(Ce)**									
Analysis #	1	2	3	4	5	6	7	8	9	10
TiO_2	43.46	43.92	42.85	32.17	33.54	34.02	31.16	33.62	32.54	33.99
Fe_2O_3	3.13	2.18	4.23	3.26	6.2	3.21	3.21	3.21	6.22	3.29
SiO_2	0.07	0.11	0.09	0.76	0.25	0.35	0.43	0.38	0.14	0.43
MnO	1.25	0.9	0.82	<0.04	<0.04	<0.04	<0.04	<0.04	<0.04	<0.04
Nb_2O_5	0.27	0.3	0.26	12.93	9.25	10.95	13.77	11.03	10.85	9.92
Ta_2O_5	0.0	0.0	0.0	0.11	0.06	0.05	0.12	0.06	0.08	0.08
CaO	0.76	0.68	1.18	2.09	1.58	1.56	1.99	1.46	1.55	1.83
ZrO_2	0.25	0.17	0.24	1.5	2.4	2.08	1.48	2	1.9	2.11
Y_2O_3	0.09	0.06	0.06	4	3.27	5.2	5.66	5.52	2.9	4.69
La_2O_3	13.62	14.18	14.01	6.18	5.44	5.62	5.07	5.29	5.4	5.42
Ce_2O_3	21.31	21.74	20.63	17.13	16.34	14.8	15.64	14.43	16.94	14.6
Pr_2O_3	1.47	1.66	1.44	2.07	1.97	1.93	1.75	1.82	2.27	1.86
Nd_2O_3	4.42	4.48	4.19	7.79	8.18	8.35	7.98	8.34	8.83	8.16
Sm_2O_3	0.48	0.46	0.43	1.12	1.41	1.83	1.42	2.12	1.86	1.88
Eu_2O_3	0.11	bdl	0.22	0.47	1.16	0.95	0.54	0.88	1.27	0.88
Gd_2O_3	0	0.13	0.13	0.88	1.45	1.89	1.19	1.97	1.75	1.87
Dy_2O_3	0.21	0.15	0	0.58	0.87	1.1	0.71	1.33	0.84	1.01
Yb_2O_3	<0.11	<0.11	<0.11	<0.11	<0.11	<0.11	<0.11	<0.11	<0.11	<0.11
Er_2O_3	<0.13	0.19	<0.13	<0.13	<0.13	<0.13	<0.13	<0.13	<0.13	<0.13
H_2O	2.97	2.84	3.15	2.44	2.69	2.39	2.21	2.38	2.64	2.48
F	0.46	0.42	0.33	0	0.3	0.23	0.34	0.19	0.34	0.22
Total	94.18	94.45	94.2	95.48	96.23	96.42	94.53	95.94	98.17	94.63
Formulae based on 3 cations										
Si	0.004	0.006	0.005	0.045	0.015	0.020	0.025	0.022	0.008	0.025
Ti	1.868	1.897	1.833	1.410	1.450	1.480	1.385	1.472	1.400	1.495
Fe^{3+}	0.135	0.094	0.181	0.143	0.268	0.140	0.143	0.141	0.268	0.145
Nb	0.007	0.008	0.007	0.341	0.240	0.286	0.368	0.290	0.281	0.262
Ta	0.000	0.000	0.000	0.002	0.001	0.001	0.002	0.001	0.001	0.001
Cat_B	2.014	2.005	2.026	1.939	1.974	1.927	1.923	1.925	1.958	1.928
Ca	0.047	0.042	0.072	0.130	0.098	0.097	0.126	0.091	0.095	0.115
Mn	0.060	0.044	0.040	0.000	0.000	0.000	0.000	0.000	0.000	0.000
Y	0.003	0.002	0.002	0.124	0.100	0.160	0.178	0.171	0.088	0.146
Zr	0.007	0.005	0.007	0.043	0.067	0.059	0.043	0.057	0.053	0.060
La	0.287	0.300	0.294	0.133	0.115	0.120	0.110	0.113	0.114	0.117
Ce	0.446	0.457	0.429	0.365	0.344	0.313	0.337	0.308	0.354	0.312
Pr	0.031	0.035	0.030	0.044	0.041	0.041	0.038	0.039	0.047	0.040
Nd	0.090	0.092	0.085	0.162	0.168	0.172	0.168	0.173	0.180	0.171
Sm	0.009	0.009	0.009	0.022	0.028	0.037	0.029	0.042	0.037	0.038
Eu	0.002	0.000	0.004	0.009	0.023	0.019	0.011	0.017	0.025	0.018

Table 1Contd.....…

Gd	0.000	0.002	0.002	0.017	0.028	0.036	0.023	0.038	0.033	0.036
Dy	0.004	0.003	0.000	0.011	0.016	0.021	0.014	0.025	0.016	0.019
Er	0.000	0.004	0.000	0.000	0.000	0.000	0.000	0.000	0.000	0.000
Yb	0.000	0.000	0.000	0.000	0.000	0.000	0.000	0.000	0.000	0.000
Cat_A	0.986	0.995	0.974	1.061	1.026	1.073	1.077	1.075	1.042	1.072
F	0.083	0.076	0.059	0	0.055	0.041	0.064	0.035	0.062	0.041
OH	1.131	1.086	1.195	0.949	1.029	0.923	0.871	0.924	1.008	0.966
O'	4.786	4.838	4.746	5.052	4.916	5.036	5.066	5.042	4.93	4.993
REE	0.869	0.902	0.853	0.764	0.762	0.758	0.731	0.756	0.806	0.750
REE+Y	0.872	0.904	0.855	0.888	0.862	0.918	0.909	0.927	0.894	0.896
REE_2O_3	41.62	42.99	41.05	36.22	36.81	36.47	34.3	36.16	39.14	35.68

Type	**Aeschynite-(Ce)**							**Nb-aeschynite-(Ce)**			
Analysis #	11	12	13	14	15	16	17	18	19	20	21
TiO_2	32.0	34.93	35.99	36.37	36.57	33	25.6	16.96	13.61	17.96	14.97
Fe_2O_3	5.84	5.25	4	4.02	2.51	3.84	6.64	3.83	4.46	4.45	4.05
SiO_2	0.22	0.42	0.26	0.25	0.16	0.2	0.18	0.15	0.15	0.16	0.19
MnO	<0.04	<0.04	0.13	0.11	0.07	0.07	<0.04	<0.04	<0.04	0.09	<0.04
Nb_2O_5	11.49	7.58	8.61	7.84	9.31	12.34	19	30.75	33.1	28.77	31.84
Ta_2O_5	0.09	0.08	0.08	0.05	0.12	0.19	0.16	0.54	0.81	0.49	0.77
CaO	1.52	1.58	1.78	1.81	1.73	1.88	1.48	1.95	2.2	2.16	2.19
ZrO_2	2.09	2.57	1.67	1.6	1.89	1.48	1.78	2.15	2.49	2.18	2.41
Y_2O_3	3.15	3.59	6.27	5.74	1.93	3.8	3.62	3.18	2.58	4.63	2.94
La_2O_3	5.25	5.22	4.51	5.13	9.59	6.29	4.19	3.61	4.24	2.6	4.14
Ce_2O_3	16.72	16.01	16.09	16.45	18.69	17.96	14.53	13.89	14.42	10.98	14.19
Pr_2O_3	2.17	2.03	2.07	1.89	1.93	2.08	2.14	1.99	1.94	1.83	2.01
Nd_2O_3	8.44	8.26	7.75	7.48	7.46	7.73	8.54	8.61	7.9	8.28	7.93
Sm_2O_3	1.67	1.47	1.35	1.14	0.95	1.12	1.89	2.22	1.77	3.15	1.59
Eu_2O_3	1.2	1.21	0.71	0.59	0.31	0.4	1.33	1.16	0.9	1.46	0.93
Gd_2O_3	1.73	1.48	1.24	1.16	0.41	0.81	1.89	1.88	1.46	3.1	1.49
Dy_2O_3	1.01	1.01	0.76	0.67	0.18	0.51	1.06	1.26	0.88	1.8	0.95
Yb_2O_3	<0.11	<0.11	0.19	0.2	0.14	0.16	<0.11	<0.11	<0.11	0.17	<0.11
Er_2O_3	<0.13	<0.13	0.36	0.29	0.07	0.15	<0.13	<0.13	<0.13	0.43	<0.13
H_2O	2.55	2.68	2.7	2.75	2.37	2.37	2.13	1.07	0.95	1.32	0.86
F	0.26	0.35	0.34	0.28	0.36	0.34	nd	nd	nd	0.21	0.29
Total	97.31	95.57	96.71	95.7	96.6	96.59	96.15	95.19	93.84	96.12	93.63

Table 1. Contd….

Formulae Based on 3 Cations											
Si	0.013	0.024	0.015	0.014	0.009	0.012	0.011	0.009	0.010	0.010	0.013
Ti	1.389	1.512	1.532	1.558	1.584	1.437	1.151	0.813	0.669	0.843	0.732
Fe^{3+}	0.254	0.227	0.170	0.172	0.109	0.167	0.299	0.184	0.219	0.209	0.198
Nb	0.300	0.197	0.220	0.202	0.242	0.323	0.513	0.886	0.978	0.812	0.936
Ta	0.001	0.001	0.001	0.001	0.002	0.003	0.003	0.009	0.014	0.008	0.014
Cat_B	1.957	1.961	1.938	1.947	1.946	1.942	1.976	1.901	1.890	1.883	1.892
Ca	0.094	0.097	0.108	0.111	0.107	0.117	0.095	0.133	0.154	0.144	0.152
Mn	0.000	0.000	0.006	0.006	0.003	0.003	0.000	0.000	0.000	0.005	0.000
Y	0.097	0.110	0.189	0.174	0.059	0.117	0.115	0.108	0.090	0.154	0.102
Zr	0.059	0.072	0.046	0.045	0.053	0.042	0.052	0.067	0.079	0.066	0.076
La	0.112	0.111	0.094	0.108	0.204	0.134	0.092	0.085	0.102	0.060	0.099
Ce	0.353	0.337	0.333	0.343	0.394	0.381	0.318	0.324	0.344	0.251	0.338
Pr	0.046	0.043	0.043	0.039	0.041	0.044	0.047	0.046	0.046	0.042	0.048
Nd	0.174	0.170	0.157	0.152	0.154	0.160	0.182	0.196	0.184	0.185	0.184
Sm	0.033	0.029	0.026	0.022	0.019	0.022	0.039	0.049	0.040	0.068	0.036
Eu	0.024	0.024	0.014	0.012	0.006	0.008	0.027	0.025	0.020	0.031	0.021
Gd	0.033	0.028	0.023	0.022	0.008	0.016	0.037	0.040	0.032	0.064	0.032
Dy	0.019	0.019	0.014	0.012	0.003	0.010	0.020	0.026	0.019	0.036	0.020
Er	0.000	0.000	0.006	0.005	0.001	0.003	0.000	0.000	0.000	0.008	0.000
Yb	0.000	0.000	0.003	0.004	0.003	0.003	0.000	0.000	0.000	0.003	0.000
Cat_A	1.043	1.039	1.062	1.053	1.054	1.058	1.024	1.099	1.110	1.117	1.108
F	0.048	0.064	0.062	0.050	0.066	0.062	0.000	0.000	0.000	0.041	0.059
OH	0.982	1.029	1.018	1.044	0.910	0.916	0.850	0.453	0.413	0.548	0.374
O'	4.970	4.907	4.921	4.906	5.025	5.022	5.150	5.547	5.588	5.411	5.568
REE+Y	0.890	0.870	0.902	0.893	0.891	0.897	0.878	0.899	0.877	0.902	0.879
REE_2O_3	38.2	36.68	35.02	35	39.73	37.21	35.56	34.63	33.49	33.79	33.24

Table 2. Average of Sal Aeschynite-Ce and Nb-Aeschynite-(Ce) in Comparison to Aeschynite-(Y) from (1) Evje-Iveland, Norway [8] , (2) Triolet Valley, Italy [5], (3) Nb-Aeschynite-(Ce) from Bayan Obo, China [3] , (4) Nb-Aeschynite-(Ce) from Alaska [5]

Location	Sal (Oman)		(1)	(2)	(3)	(4)
Aeschynite-	(Ce)	Nb-(Ce)	(Y)	(Y)	Nb-(Ce)	Nb-(Ce)
Number of samples	23	4	4	11	8	1
TiO_2	34.96	15.87	35.76	45.66	21.82	20.2

Table 2. Contd….

Fe_2O_3	4.25	4.2	0.55	NR	0.27	1.09
SiO_2	0.28	0.16	NR	NR	0.11	3.51
MnO	0.19	0.02	NR	NR	NR	NR
ZrO_2	1.65	2.31	NR	NR	NR	NR
CaO	1.56	2.12	0.58	0.32	1.61	4.52
Y_2O_3	3.49	3.33	16.17	20.98	1.56	0.82
La_2O_3	6.99	3.65	0.05	0.04	1.86	4.9
Ce_2O_3	17.02	13.37	0.36	0.45	13.4	15.8
Pr_2O_3	1.92	1.54	0.14	0.12	2.64	1.9
Nd_2O_3	7.48	8.18	0.99	1.18	13.54	5.6
Sm_2O_3	1.33	2.18	1.13	0.62	2.59	NR
Eu_2O_3	0.74	1.11	NR	NR	NR	NR
Gd_2O_3	1.19	1.98	3.02	3.87	1.61	NR
Dy_2O_3	0.71	1.22	3.4	3.71	0.58	NR
Er_2O_3	0.06	0.11	2.02	2.11	0	NR
Yb_2O_3	0.04	0.04	1.88	1.53	0	NR
Nb_2O_5	9.16	31.12	12.53	3.59	36.68	47
Ta_2O_5	0.08	0.65	3.05	0.31	NR	0.1
H_2O	2.58	1.04	NR	NR	NR	NR
F	0.28	0.25	NR	NR	0.13	NR
Total	95.84	94.82	98.44	97.6	99.09	106
Total REE	37.48	33.79	12.98	13.63	36.21	NR
NR: not reported						

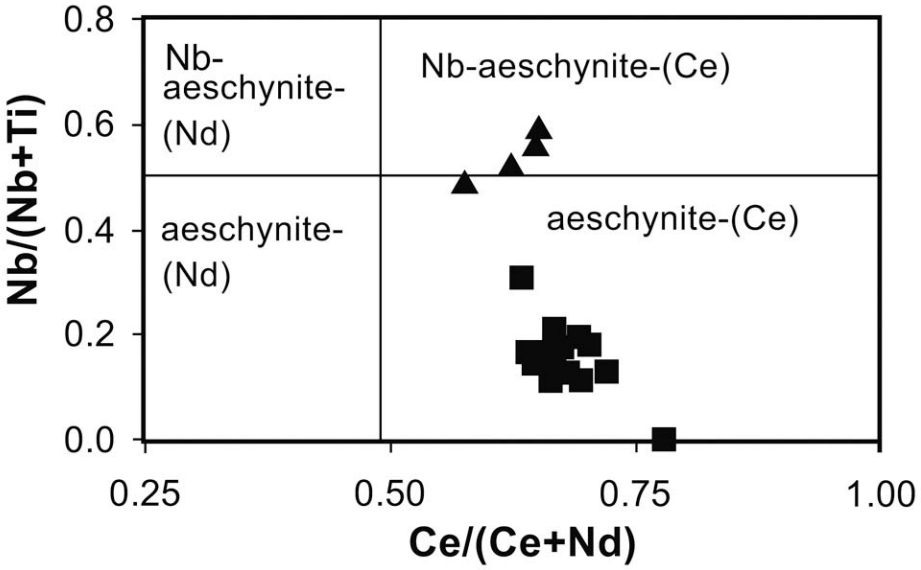

Fig. (5). Nb/(Nb+Ti) *versus* Ce/(Ce+Nd) plot of aeschynite group minerals from the Sal carbonatite.

Table 3. The Correlation Coefficients Between Analysed Cations in Aeschynite

	Ti	Fe^{3+}	Ca	Zr	Nb
Fe^{3+}	-0.39	1.0	0.17	0.49	0.27
Ca	-0.85	0.17	1.0	0.73	0.84
Mn	0.58	-0.4	-0.72	-0.86	-0.50
Zr	-0.75	0.49	0.73	1.0	0.68
Y	-0.34	0.06	0.56	0.54	0.29
La	0.66	-0.49	-0.75	-0.86	-0.62
Ce	0.64	-0.37	-0.66	-0.78	-0.57
Eu	-0.69	0.75	0.48	0.81	0.59
Sm	-0.78	0.37	0.64	0.73	0.74
Gd	-0.71	0.46	0.59	0.76	0.65
Dy	-0.72	0.4	0.57	0.75	0.67
Er	-0.02	-0.17	0.12	-0.11	0.04
Ta	-0.91	0.17	0.76	0.55	0.94
Nb	-0.99	0.27	0.84	0.68	1.0
OH	0.95	-0.13	-0.83	-0.62	-0.98
REE +Y	-0.05	-0.51	0.12	0.03	0.09
Yb	0.01	-0.19	0.23	-0.02	0.0
Pr	-0.73	0.53	0.66	0.77	0.67
Nd	-0.77	0.46	0.76	0.92	0.7

The presence of Ca substituting for REE also requires charge balance consideration. Because of the clear negative correlation with Ti (Table **3**, Fig. **6a**), the coupled substitution $Ti_1(REE)_1Nb_{-1}$ Ca_{-1} is likely, as already proposed by Yang *et al.* [3].

It is not easy to assess a substitution mechanism for Zr which is present in small quantities only (up to 0.1 a.p.f.u.). A negative correlation with Ti suggests a substitution like $Zr_{-1}Ti_{-1}$ $Nb_1(REE)_1$. Alternatively, Zr may be coupled with OH into an exchange vector such as $Zr_{-1}O_{-1}(REE)_1(OH)_1$, however, a negative Zr-OH correlation is not discernable.

The average of aeschynites from the Sal carbonatite is given in Table **2** in comparison with other aeschynites from the world. The Sal aeschynite-Ce and Nb-aeschynite-(Ce) have high TiO_2, La_2O_3, Ce_2O_3, and Nd_2O_3 content, similar to Nb-aeschynite-(Ce) from Bayan Obo, China [3] and Nb-aeschynite-(Ce) from Alaska [5] (Table **2**). However, the aeschynites from China and Alaska have higher Nb_2O_5 content. In comparison to aeschynite-(Y) from Evje-Iveland, Norway [8] and from Triolet Valley, Italy [5], the Sal aeschynites have lower Y_2O_3 (Table **2**). The Sal aeschynites show relatively similar steep patterns with a strong enrichment of LREE in chondrite-normalized REE patterns (Fig. **8**), similar to the REE pattern of Nb-aeschynite-(Ce) from the Bayan Obo, China [3]. In contrast, the pattern for aeschynite-(Y) from Norway [9], and from the Triolet Valley, from the Western Alps [8] is flatter with less pronounced enrichment of LREE. Ti-rich aeschynites from the Western Alps and Norway have Y and HREE largely pre-

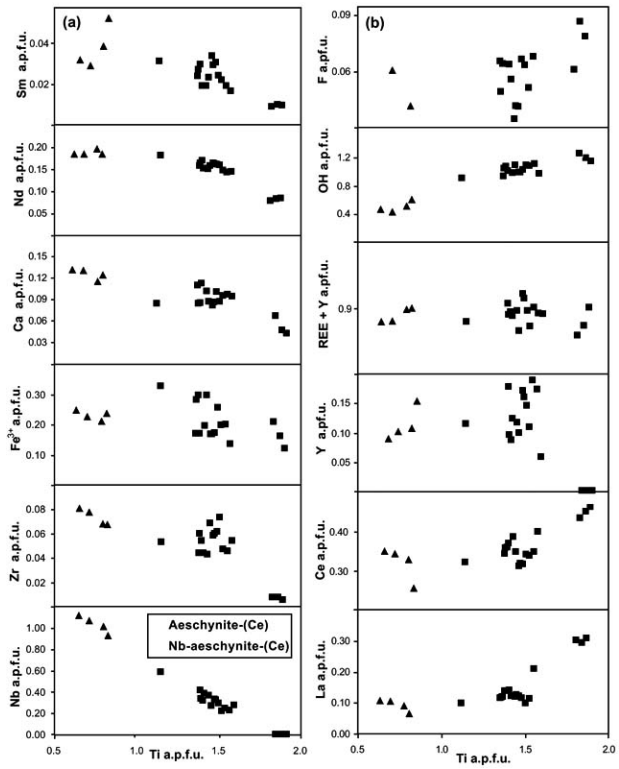

Fig. (6a.b.). Correlations (atoms per formula unit) of Ti *versus* other cations in aeschynite-group minerals from the Sal carbonatite.

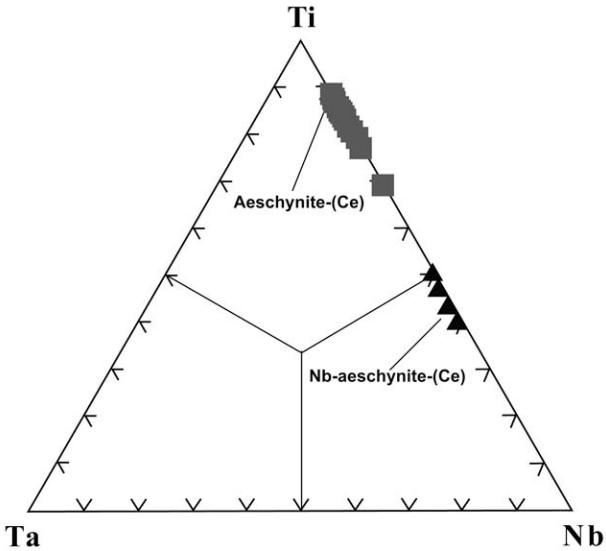

Fig. (7). Diagrammatic representation of the cation population in the B-site.

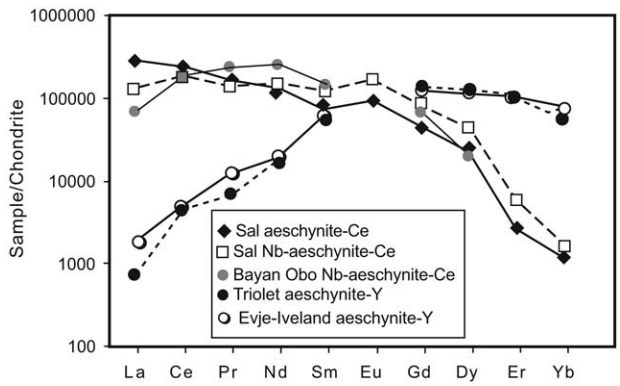

Fig. (8). Chondrite-normalized REE distribution of average REE content in aeschynites from the Sal carbonatite in comparison to average REE content in aeschynite-(Y) from Evje-Iveland, Norway [9] , Triolet Valley, Italy [8] , and niobio-aeschynite-(Ce) from Bayan Obo, China [3]. (Chondrite values from Sun and McDonough [23]).

vailing on LREE. Most studies on the compositional variation of the aeschynite-group minerals indicate that the compositional variations in these minerals were controlled by geochemical factors, fluid composition and crystal chemistry [e.g. 3,8, 9].

The formation of aeschynite-(Ce) and niobo-aeschynite-(Ce) in the Sal carbonatite is probably related to late stage of fluid activities occurred after intrusion of the carbonatite, because they coexist with barite, strontianite and thorianite as interstitial accessory minerals within the dolomite groundmass or grew on the surface of altered magnetite and Nb-rutile. These minerals could be a product of the late stage alteration of the primary mineral assemblages of the carbonatite (Sr-rich apatite, dolomite, calcite, and Ti-magnetite, Nb rutile). During the alteration process, REE, Y, Nb, and Sr may have been selectively removed from apatite , while Nb, Ti and Fe were removed from Ti-magnetite and Nb rich rutile. A similar alteration process has been experimentally investigated by Pöml et al. [22], who observed hydrothermal (250°C) formation of aeschynite at the expense of pyrochlore (betafite). However, pyrochlore was not identified in the Sal carbonatite. Accordingly, the REE and other elements enrichment were introduced by late stage fluid activities. Th and U formed thorianite, Sr and Ba formed strontianite and barite, while Nb, REE and Ti formed aeschynites.

ACKNOWLEDGEMENTS

This work was supported by research projects of Sultan Qaboos University HM grant SR/SCI/ETHS/06/01. The authors are grateful to Hans-Jürgen Bernhard, Ruhr-Universität-Bochum, for providing us a pre-version of his mineral formula calculation software “Mincalc”. W. Witte (ZSW Stuttgart) is thanked for his help with the micro Raman spectroscopic analyses. We thank Ulrich Schussler, Paola Bonazzi, Nenad Toma#$ and anonymous reviewers for their constructive comments which considerably improved the manuscript.

REFERENCES

[1] Bonazzi, P.; Menchetti, S. Crystal chemistry of aeschynite-(Y) from the Western Alps: residual electron density on difference-Fourier map. *Eur. J. Mineral.*, **1999**, *11*, 1043.

[2] Fleischer, M. Rare earths in aeschynite-priorite series, the status of lyndochite. *Mineral. Mag.*, **1966**, *35*, 801.

[3] Yang, Z.; Smith, M.; Henderson, P.; LeBas, M.; Tao, K.; Zhang, P. Compositional variation of aeschynite-group minerals in the Bayan Obo Nb-REE-Fe ore deposit, Inner Mongolia, China. *Eur. J. Mineral.*, **2001**, *13*, 1207-1214.

[4] Miyawaki, R.; Nakai, I. Crystal structures of rare earth minerals. In: *Handbook on the Physics and Chemistry of Rare Earths;* Gschneidner, K. A. Jr; Eyring, L., Eds; Elsevier Science Publishers B. V: Amsterdam, **1993**, Vol. *16*, p. 249 .

[5] Rosenblum, S.; Mosier, E.L. Non metamict nioboaeschynite-(Ce) from Alaska. *Am. Mineral.*, **1975**, *60*, 309.

[6] Edwards, D.; Rock, N.M.S.; Taylor, W.R.; Griffin, B.J.; Ramsay, R.R. Mineralogy and petrology of the Aries diamondiferious kimberlite Pipe, ventral kimberley block, Western Australia. *J. Petrol.*, **1992**, *33*, 1157.

[7] Chao, E.C.T.; Back, J.M.; Minkin, J.A.; Tatsumoto, M.; Wang, J.; Conrad, J.E.; MaKee, E.H.; Hou, Z.; Meng, Q.; Huang, S. The sedimentary carbonate-hosted giant bayan obo REE-Fe-Nb ore deposit of Inner compositional variation of aeschynite in bayan obo, Mongolia, China: a cornerstone example for giant polymetallic ore deposits of hydrothermal original. U.S. *Geol. Surv. Bull.*, **1997**, *2143*, p. 65.

[8] Bonazzi, P.; Magnanelli, S. Non-metamict Ti-rich aeschynite-(Y) from the triolet valley (Western Alps, Italy). *Neues Jahrbuch Mineral. Mh.*, **1994**, *6*, 275.

[9] Bonazzi, P.; Zoppi, M.; Dei, L. Metamict aeschynite-(Y) from the Evje-Iveland district (Norway): heat-induced recrystallization and dehydration. *Eur. J. Mineral.*, **2002**, *14*, 141-150.

[10] Skoda, R.; Novak M.Y. REE, Nb, Ta, Ti-oxide (AB2O^) minerals from REL-REE euxenite-subtype pegmatites of the trebec pluton, Czech Republic; substitutions and fractionation trends. *Lithos*, **2007**, *95*, 43.

[11] Nasir, S.; Al-Khirbash, S.; Rollinson, H. Al-Harthy Ab, A.; Al-Sayigh, A.; Al-Lazki, A.; Belousova, E.; Kaminsky, F.; Theye, T.; Massonne, H.J.; Al-Busaidi, S. *Evolved Carbonatitic Kimberlites from the Batain Nappes, Eastern Oman Continental Margin.* 9th Kimberlite Conference. **2008**, Extended abstract Nr 91KC-A-00002.

[12] Nasir, S.; Al-Khirbash, S.; Rollinson, H.; Al-Harthy Ab, A.; Al-Sayigh, A.; Al-Lazki, A.; Belousova, E.; Kaminsky, F.; Theye, T.; Massonne, H.J.; Al-Busaidi.S. *Late Jurassic to Tertiary Kimberlite, Carbonatite and Lamproite Dike Swarms from the Bomethra Area, Northeastern Oman*. 9th Kimberlite Conference. **2008**, Extended abstract Nr. 91KC-A-00003´.

[13] Mann, A.; Hanna, S.; Nolan, S.C. The post-campanian structural evolution of the central Oman mountains: tertiary extension of the

east arabian margin. In: *The Geology and Tectonics of the Oman Region.* Oman, 1990; Robertson, A.H.F.; Searle, M.P.; Ries, A. Eds.; Geological society: London, Special Publication, **1990**, Vol. *49*, p. 549.

[14] Loosveld, R.; Bell, A.; Terken J. The tectonic evolution of Interior Oman. *GeoArabia*, **1996**, *1* , 28.

[15] Worthing, M.; Nasir, S.; Cambro-ordovician potassic (alkaline) magmatism in central Oman: Petrological and geochemical constraints on petrogenesis. *Lithos*, **2008**, *106*, 25.

[16] Lapierre, H.; Samper, A.; Bosch, D.; Maury, R.C.; Bechennec, F.; Cotton, J.; Demant, A.; Brunet, P.; Keller, F.; Marcoux, J. The tethyan plume: geochemical diversity of middle permain basalts from the Oman rifted margin. *Lithos*, **2004**, *74*,167.

[17] Reed, S.J.B.; Buckley A. Rare-earth element determination in minerals by electron-probe microanalysis: application of spectrum synthesis. *Mineral. Mag*., **1998**, *62*, 1.

[18] Ecrit, T.S. Identification and alteration trends of granitic-pegmatite-hosted (Y, REE, U, Th) - (Nb,Ta,Ti) oxide minerals: a statistical approach. *Can. Mineral.*, **2005**, *43*, 1291.

[19] Gieré, R.; Williams, C.T. REE-bearing minerals in a Ti-rich vein from the adamello contact aureole; Italy. *Contrib. Mineral. Petrol.*, **1992**, *112*, 83.

[20] Bayliss, P.; Levinson, A.A. a system of nomenclature for rare-earth mineral species: revision and extension. *Am. Mineral.*, **1988**, *73*, 422.

[21] Nickel, E.H.; Grice, J.D. The IMA commission of new minerals and mineral names: procedures and guidelines on mineral nomenclature. *Can. Mineral.*, **1998**, *36*, 913.

[22] Pöml, P.; Menneken, M.; Stephan, T.; Niedermeier, D.R.D.; Geisler, T.; Putnis, A. Mechanism of hydrothermal alteration of natural self-irradiated and synthetic crystalline titanate-based pyrochlore. *Geochem. Cosmochem. Act*., **2007**, *71*, 3311.

[23] Sun, S.S.; McDonough, W.F. In: *Chemical and Isotopic Systematics of Oceanic Basalts: Implications for Mantle Compositions and Processes;* Saunders, A.D.; Norry M.J. Eds.; *Magmatism in the Ocean Basins.* Geological Society of London, Special Publication, **1989**, Vol. *42*, pp. 313-345.

Received: March 17, 2009 Revised: May 06, 2009 Accepted: June 03, 2009